Detecting functional relationships between simultaneous time series

C. L. Goodridge, L. M. Pecora, T. L. Carroll, and F. J. Rachford
Code 6345, U.S. Naval Research Laboratory, Washington, D.C. 20375
(Received 12 September 2000; revised manuscript received March 8 2001; published 23 July 2001)

We describe a method to characterize the predictability and functionality between two simultaneously generated time series. This nonlinear method requires minimal assumptions and can be applied to data measured either from coupled systems or from different positions on a spatially extended system. This analysis generates a function statistic, Θ_{c0}, that quantifies the level of predictability between two time series. We illustrate the utility of this procedure by presenting results from a computer simulation and two experimental systems.

DOI: 10.1103/PhysRevE.64.026221 PACS number(s): 05.45.Tp, 05.10.−a

I. INTRODUCTION

A common challenge encountered by experimentalists in nonlinear dynamics is how to relate pairs of time series, such as those measured from two points on a spatially extended system or from two coupled systems. Many nonlinear systems exhibit spatial as well as temporal dynamics and an understanding of the spatial behavior is often vital to understanding the overall dynamics [1]. Examples of such spatiotemporal systems are ''auto-oscillations'' of magnetostatic spin wave modes in ferrimagnetic films [2], the response of a magnetostrictive ribbon to ac magnetic fields, and fluid motion in Taylor-Coquette flow [3] or Rayleigh-Bernard convection [4]. One way to characterize the spatial dynamics is to simultaneously monitor a property of the system at two different positions and determine the relationship between the resulting data. The relationship between simultaneous time series may also describe properties of the coupling between two coupled systems. A wide variety of linear techniques are available to investigate the functionality between concurrent time series, but these techniques often fail to provide any useful information if the relationship is nonlinear.

In this paper we will describe a general nonlinear technique that investigates the functionality between pairs of time series with minimal assumptions about the nature of either the data or the dynamics. This generality allows this technique to be applied to a wide range of experimental systems and to account for more general functionality than strictly linear. The result of this analysis is a function statistic, Θ_{c0}, that quantifies the predictability and functionality between the two time series and can be compared to results from linear techniques such as the cross correlation. This technique may be useful to experimentalists with time series data as well as provide another tool for general time series analysts.

The procedure builds on techniques designed to investigate functionality between time series [5], especially those of several of the authors [6,7]. These earlier procedures calculate statistics that quantify certain properties of functions relating time series such as continuity or differentiability. This analysis provides a way to calculate a function statistic that is a measure of the predictability between the time series. Roughly speaking, this statistic quantifies how well can we predict the behavior of one time series if we know the behavior of the other time series. This technique can be extended to investigate the nature of the functional relationship between the two time series by testing for nonlinearity in the function. One important aspect of this technique is that it uses the data to establish a limiting length scale—a limit of relevance [8]—rather than intuition or knowledge about the system. This analysis is also general enough to be applicable to both experimental and computational results.

II. PROCEDURE

Given two simultaneous time series $\{h_i, g_i\}$ [9], we construct vectors $\mathbf{x}_i$ and $\mathbf{y}_i$ and attractors $\mathbf{X}$ and $\mathbf{Y}$, such that

$$\mathbf{x}_i = (h_i, h_{i+\tau}, \ldots, h_{i+\tau*(d-1)}) \in \mathbf{X}$$

and

$$\mathbf{y}_i = (g_i, g_{i+\tau}, \ldots, g_{i+\tau*(d-1)}) \in \mathbf{Y},$$

by time delay embedding. The parameters of the embedding, the time delay τ and the embedding dimension d, are determined using the minimum of the autocorrelation function [1] and the false nearest neighbor algorithm of Abarbanel [10], respectively [11]. However, any combination of d and τ that adequately captures the dynamics of the system should yield useful results. Next we assume that a function F exists such that $\mathbf{y}_i = F(\mathbf{x}_i)$. Function F is assumed to be continuous but no other conditions are imposed. Since the determination of F may not be trivial, an intermediate goal is to investigate properties of the function. We will calculate a function statistic that allows us to describe whether function F actually exists, how accurately we can make predictions between time series, and if the function is nonlinear. To derive this statistic, we assume that nearby points on $\mathbf{X}$ map to nearby points on $\mathbf{Y}$ (see Fig. 1), provided F exists. This behavior is equivalent to the two time series being related by a continuous function. Our function statistic, Θ_{c0}, is a measure of the local predictability between the two time series. A high value indicates strong predictability between the time series.

Here is an outline of the procedure to calculate Θ_{c0}. In all of the following, we assume that we have measured the data in such a way that h_i and g_i are sampled simultaneously and we define $\mathbf{x}_i$ and $\mathbf{y}_i$ as corresponding points if the indices of the first coordinates are equal. We systematically investigate

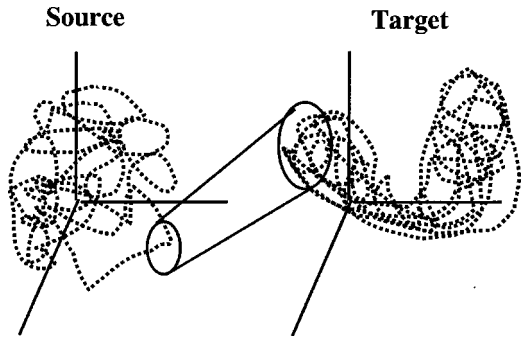

FIG. 1. This technique quantifies the behavior of corresponding points on the two time series; that is, do points, which are nearest neighbors on the source attractor, have corresponding points (simultaneous in time) which are nearest neighbors on the target attractor.

clusters of nearest neighbors on one attractor (the source), and quantify the locality of the corresponding points on the other attractor (the target) using a reference length scale σ. We utilize the variance of points on the attractors as our measurement and determine the predictability using the significance of this variance. The significance of the variance is defined as the probability that the actual variance is larger than a given variance, given a probability distribution function for the variance with σ^2 as the mean variance. Each cluster of points on the target attractor will yield a value for Θ_{c^0}. We repeat this calculation for a number of clusters and average the values to find an attractor-wide value for the function statistic. There are two primary steps in this analysis, first, to determine the reference length scale and then to calculate the function statistic. The two steps are outlined below:

(I) *Determination of length scale σ on target attractor:*

(1) Select a point (a ''center'') $\mathbf{y}_c$ on the target attractor $\mathbf{Y}$ ($\mathbf{Y}$ is generated from the g_i time series).

(2) Gather N nearest neighbors of this center, where N is large enough to achieve good statistics but small enough to calculate a minimum length scale (Fig. 2).

(3) Determine the variance of these points about $\mathbf{y}_c$.

(4) Set the significance of the variance equal 0.95 and solve for $\sigma(\mathbf{y}_c)$.

(5) Repeat for a number (N_c) of other centers on $\mathbf{Y}$ and average these results to generate an attractor-wide scale, $\sigma = 1/N_c \Sigma_{i=1}^{N_c} \sigma(\mathbf{y}_i)$.

(II) *Determination of function statistic:*

(1) Select a center $\mathbf{x}_0$ on source attractor $\mathbf{X}$.

(2) Gather all of the points within some radius δ of this center.

(3) Find all of the corresponding (i.e., simultaneous in time [12]) points on the target attractor centered around $\mathbf{y}_0$, the corresponding point of $\mathbf{x}_0$ (Fig. 3). $\mathbf{x}_0$ and $\mathbf{y}_0$ have simultaneously sampled first coordinates, i.e., h_0 and g_0, respectively.

(4) Find the variance of these points and calculate the significance of this variance $\Theta_{c^0}(\mathbf{x}_0)$.

(5) Vary δ to maximize the significance for this point.

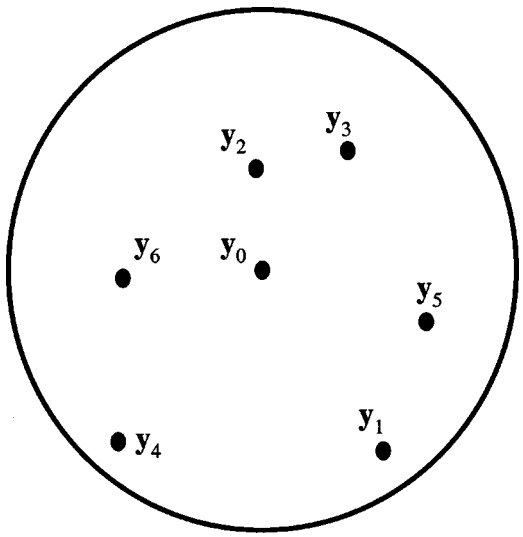

FIG. 2. The target attractor is divided into clusters of points, which are nearest neighbors to a center point. The variance of these points is used in the determination of the length scale σ.

(6) Repeat for a number of other centers on the source attractor and average to find a value for the attractor-wide function statistic.

For good predictability our null hypothesis is that σ is a typical length scale for our data, implying that sets with no functional relationship will have predictability errors $\gg \sigma$, hence resulting in low significance of variance. In actuality, we want to show that the variance is much smaller than σ and that σ acts as a good upper bound so we know prediction at error levels below σ is likely. This is the same as requiring that the variance of a cluster of points has an upper bound. High values of the significance of the variance correspond to high predictability and therefore the high likelihood that the time series are related by a function. This analysis investigates the functionality between two time series and does not seek to address whether the two time series are synchronized (i.e., one system is driving the other). The results we describe here are determined from time series generated by sampling at two points on spatially extended systems and most likely do not experience a monodirectional interaction and are examples of mutual coupling [13].

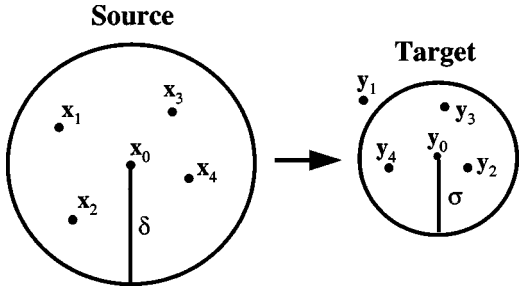

FIG. 3. Nearest neighbors on the source attractor $\mathbf{X}$ (defined as being within radius δ of a given center point $\mathbf{x}_0$) and the corresponding points on the target attractor $\mathbf{Y}$. Our statistic quantifies the locality of the corresponding points to within some length scale σ.

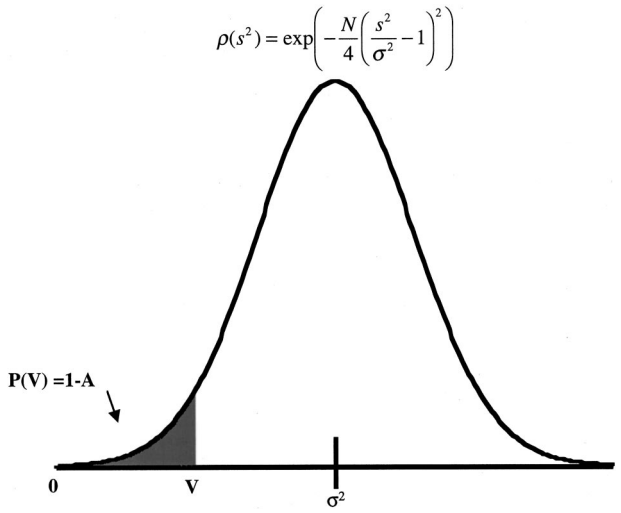

FIG. 4. We evaluate the Gaussian from $0 \rightarrow V$ to determine a value for the significance of the variance and therefore the function statistic. The normalization of the integration will depend on the mean of the distribution. *A* is the area beneath the curve.

A. Derivation of significance of variance

In order to calculate the significance of the variance for these clusters of points, we need an expression for the probability distribution function ρ for the variance, which we will determine using the central limit theorem. For any group of values, $\{s^2|s_1^2,s_2^2,s_3^2,\ldots\}$, where both the mean $\sigma^2 = (1/N)\Sigma_{i=0}^{(N-1)} s_i^2$ and the standard deviation $\gamma^2 = \langle (s_i^2 - \langle s^2 \rangle)^2 \rangle$ are known, we can approximate the $\rho(s^2)$ as $\exp[\{N(s^2-\sigma^2)/2\gamma^2\}]$ as $N \rightarrow \infty$. If the Gaussian approximation ($\gamma^2 = 2\sigma^4$) is applied, then the probability distribution function can be written as

$$\rho(s^2) = \exp\left(-\frac{N}{4}\left(\frac{s^2}{\sigma^2}-1\right)^2\right). \tag{1}$$

We then use this expression as the probability distribution function of the variance of clusters of points on attractors. The significance of the variance *P* is defined as the probability that a given variance is larger than s^2,

$$P(V) = 1 - \frac{1}{\phi}\int_0^V \exp\left(\frac{-N}{4}\left(\frac{s^2}{\sigma^2}-1\right)^2\right) ds^2, \tag{2}$$

where ϕ is the normalization constant (Fig. 4). This expression is used to calculate both the length scale σ and the function statistic Θ_{c0} (see previous section).

When using a Gaussian for the probability distribution function of a set of variances, we need to account for the possibility of unphysical negative variances. We account for this by integrating from $0 \rightarrow V$, truncating the negative variances, and by modifying the normalization constant. If the mean of the distribution is far from 0, then $\phi \rightarrow 2$. On the other hand, as the mean of the distribution approaches 0, then $\phi \rightarrow 1$. To find the normalization constant, we set

$$\frac{1}{\phi}\int_0^V \exp\left(-\frac{N}{4}\left(\frac{s^2}{\sigma^2}-1\right)^2\right) ds^2 = 1 \quad \text{as} \quad V \rightarrow \infty \tag{3}$$

to find that $\phi = 1 + E_f(\sqrt{N}/2)$, E_f is the error function. This expression for the normalization constant accounts for the truncation of negative variance values.

B. Scale determination

One strength of this analysis is that we calculate a length scale from the data themselves without making any assumptions about the dynamics. The attractors allow us to determine a scale σ directly from the data. Here is the procedure. Select a randomly determined point $\mathbf{y}_c$ (the center) on the target attractor $\{\mathbf{y}|\mathbf{y}_0,\mathbf{y}_1,\mathbf{y}_2,\mathbf{y}_3,\ldots\}$. Gather the *N* nearest neighbors of center $\mathbf{y}_c$ and calculate the variance of these points,

$$V = \frac{1}{N-1}\sum_{j=1}^{N} (y_j - \overline{y})^2, \tag{4}$$

where $\overline{y}$ is the mean. A Theiler exclusion [14] is used to avoid counting points that are very close in time as nearest neighbors. Each cluster of points will contain a specified number of points, large enough to achieve good statistics but small enough to produce a minimum length scale. The number of points *N* has ranged from 20 to 50 points to 1–2 % of the total number of points, depending on the nature of the data (considering factors such as noise and the total number of points).

To determine a value for σ, we insert this variance into the equation for the significance of the variance, set the significance equal to 0.95, and determine the corresponding σ. Repeat for a number of randomly determined centers N_c and average the values to produce an attractor-wide scale σ,

$$\sigma = \frac{1}{N_c}\sum_{i=1}^{N_c} \sigma(\mathbf{y}_i). \tag{5}$$

The resulting value is based solely on the data without any *a priori* assumptions about the system dynamics. We now use this scale to calculate the function statistic. For the cases described here we have used 100 points and therefore calculated 100 variance values, which allows us to be confident that our probability distribution function for the variance is a normal distribution [15].

C. Calculation of function statistic

Given scale σ on the target attractor, we now turn to the source attractor $\{\mathbf{x}|\mathbf{x}_0,\mathbf{x}_1,\mathbf{x}_2,\mathbf{x}_3,\ldots\}$. To begin the function statistic calculation, we gather all of the points within some radius δ of some randomly selected center on this attractor $\mathbf{x}_0$, $\{\mathbf{x}_0|\mathbf{x}_1,\mathbf{x}_2,\mathbf{x}_3,\ldots\}$. (In this case the indices of these points refer to the spatial neighbors of $\mathbf{x}_0$, not the temporal order of the time series.) The variance and significance of the corresponding points on the target attractor $\{\mathbf{y}_0|\mathbf{y}_1,\mathbf{y}_2,\mathbf{y}_3,\ldots\}$ are then calculated. δ is then varied on the source attractor (Fig. 5) to maximize the $P(V)$ for this center,

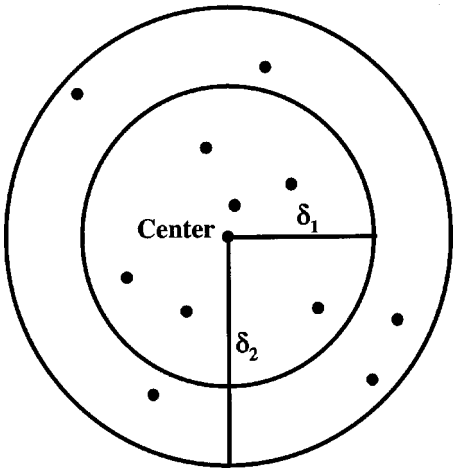

FIG. 5. The radius is varied around a given center and the variance of each collection of points is calculated. The number of points used to determine the length scale σ varies depending on the nature of data.

$$\Theta_{c^0}(x_0) = \overset{\max}{\delta}\{P(x_0)\}. \tag{6}$$

This is roughly a measure of the percentage of points on the first attractor whose corresponding points fall within σ around $\mathbf{y}_0$ on the target attractor. The function statistic Θ_{c^0} is defined as the average of $\Theta_{c^0}(x_0)$ for a number of clusters across the attractor:

$$\Theta_{c^0} = \frac{1}{N_c}\sum_{i=1}^{N_c} \Theta_{c^0}(\mathbf{x}_i), \tag{7}$$

where N_c is the number of centers. Again, we use at least 100 points to achieve good statistics [15]. High values for the function statistic indicate that good predictability and strong functionality exist; low values indicate that it is unlikely that the two time series are related by a function.

D. Function statistic beyond linear

Another application of this analysis is to use this statistic to test for nonlinearity in the functional relationship between two time series. The function statistic beyond linear is a measure of how much more accurate a nonlinear prediction is than a strictly linear prediction. The procedure for this application is this:

(1) Fit the attractors to a linear model: $\mathbf{Y} = A\mathbf{X}$. We have used a least squares fit model in the analysis presented here.

(2) Determine the variance of the residues

$$\eta = \sum (\mathbf{y}_i - A\mathbf{x}_i)^2. \tag{8}$$

(3) Use this value η for the scale σ in the significance calculation.

If there is only a linear relationship between the two attractors, η and σ are on the same order and the values for the function statistic beyond linear are low. If there are nonlinear components to the relationship between the time series, then $\eta > \sigma$ and the values for the function statistic are high. Care must be taken when using this analysis and it should only be utilized when a relationship is believed to exist between the two time series. Two completely stochastic time series will produce a large value for the variance of the residues and the calculated statistic may also be high, indicating functionality when none exists. We now present results from several experimental systems.

II. ROSSLER FORCED LORENZ SIMULATION

We will first apply this technique to data from a computer simulation to verify that we generate the expected results. We will use a six-dimensional system consisting of a Lorenz system driven by a Rossler system:

$$\text{Rossler drive} \quad \begin{cases} \dot{X}_R = -(Y_R + Z_R) \\ \dot{Y}_R = X_R + aY_R \\ \dot{Z}_R = b + Z_R(X_R - c), \end{cases} \tag{9}$$

$$\text{Lorenz response} \quad \begin{cases} \dot{X}_L = -\sigma(X_L - Y_L) \\ \dot{Y}_L = -X_L Z_L + \rho X_L - Y_L + K(\gamma Y_R - Y_L), \quad K = \text{coupling constant} \\ \dot{Z}_L = X_L Y_L - \beta Z_L, \end{cases} \tag{10}$$

where $a = b = 0.2$, $c = 0.7$, $\sigma = 10$, $\beta = 8/3$, and $\rho = 60$. In order to make the two systems comparable we select $\gamma = 3.0$ as the gain constant, which makes the Rossler amplitude comparable to the Lorenz amplitude and tune the time steps to make the two time scales comparable.

We present three sets of data where we determine the predictability from the Rössler time series to the Lorenz time series. The data are simultaneous measurements of the Rossler X coordinate and the Lorenz X coordinate. The first set has no additive noise and no coupling, the second set has no additive noise and strong coupling ($K = 0.4$), and the third set has 5% additive noise and strong coupling ($K = 0.4$). Values for the cross correlation, function statistic, and function statistic beyond linear for each of these states

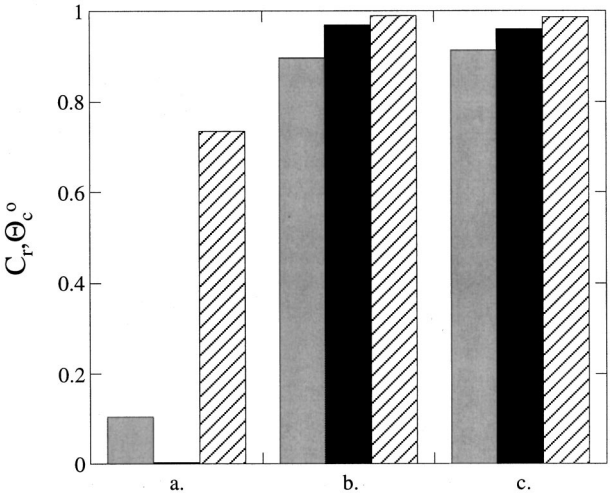

FIG. 6. A plot showing three different statistics, the cross correlation (gray fill), the function statistic (black), and the function statistic beyond linear (crosshatch), for the Rossler driven Lorenz system. The three cases are (a) no coupling, no noise, (b) 40% coupling, no noise, and (c) 40% coupling, 5% noise. The high values for the cases with coupling indicate that there is a functional relationship between the two time series, likely nonlinear in nature considering the high values for the nonlinear statistic.

are shown in Fig. 6. The cross-correlation and the function statistic are low for the uncoupled case, which is consistent for two independent systems. The lack of any linear relationship implies a large value for the variance of the residues and explains the higher value for the function statistic beyond linear.

The high values for the three statistics indicate that the two time series have strong predictability and are strongly related by a function for the two coupled cases. The addition of 5% noise has a very slight (1% or 2% change) effect on the two statistics. The high value for the function statistic beyond linear for both coupled cases indicate that the function relating the two time series may have nonlinear components.

III. SPIN WAVES IN YTTRIUM IRON GARNET FILMS

A solid state system that exhibits spatial-temporal chaotic dynamics is spin wave modulation of resonant modes in yttrium iron garnet (YIG) films. YIG is a technologically useful ferrimagnetic material used in microwave devices such as limiters, resonators, and filters and many aspects of its nonlinear behavior have been studied and exploited [16]. A number of previous experiments performed by several of the authors [17–20] have investigated the global temporal dynamics of YIG structures. In our experiments, we analyze the magnetic response at two positions on the surface of a YIG film to investigate the spatial dynamics across the film.

When YIG films are placed in saturating dc magnetic fields, the atomic spins initially align and precess around the direction of the dc field. Unless the spins are excited by an ac magnetic field, the spin precessions will damp out. When a resonant ac magnetic field is applied perpendicularly to the

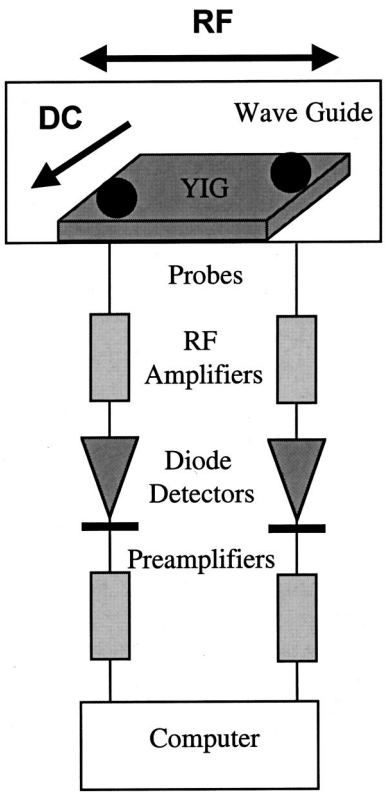

FIG. 7. Coaxial probes measure the magnetic moment of the YIG film at two positions. A pair of diode detectors then measures the modulation of the spin waves.

dc field, the spins will precess around the dc field direction at the resonant frequency [21]. Phase modulations in the processions of neighboring spins produce traveling spin waves which, when reflected at the film boundaries, result in standing waves corresponding to the magnetostatic modes of the film. At low applied ac powers, these modes are linear at the resonant frequency but are coupled to initially negligible nonlinear modes. As the excitation power is increased above a threshold power (the Suhl instability) [16], the linear modes begin to interact with continuum half-frequency spin waves in the film. The nonlinear interaction of the stationary modes and the half-frequency spin wave manifold produce nonlinearities that eventually dominate the dynamics. These interactions lead to low frequency (kHz) modulations of the amplitude of the (GHz) magnetostatic mode resonances. These modulations have been observed in both small spheres and thin films of YIG. These modulations are measured in our experiments and can exhibit periodic (called auto-oscillations), quasiperiodic, and chaotic behavior.

A diagram of the experiment can be seen in Fig. 7. Our sample is a rectangular film cut from a single YIG crystal with dimensions $0.85 \times 0.72\,\mathrm{cm}^2$ and is 37 μm thick. The modulations of the magnetostatic modes are detected by using a pair of coaxial probes mounted near the film surface. The film is mounted in a waveguide and is excited by a 2–4 GHz microwave field. The probes are oriented to pick up the resonant oscillation of the magnetization in the film. The probe microwave field is amplified and detected using standard diode detectors. The kHz auto-oscillation modulation is

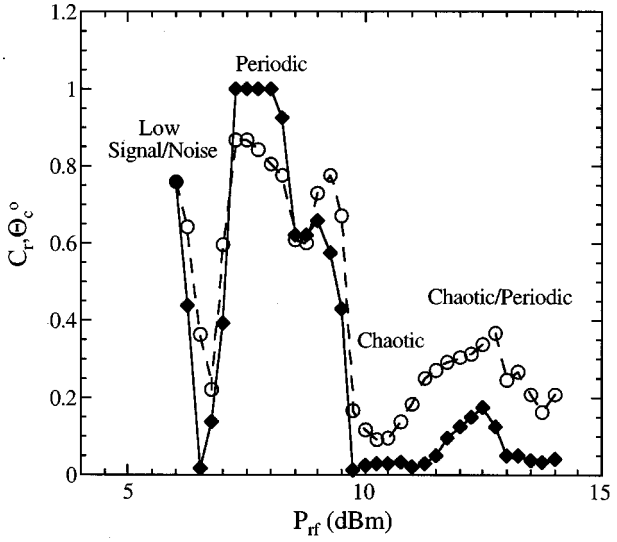

FIG. 8. This plot shows the maximum value for the cross correlation (○) and the function statistic (◆) for a power sweep performed at dc field 460.1 G and excitation frequency 3.0251 GHz, plotted against radio frequency power P_{rf}. The linear cross correlation and the nonlinear function statistic exhibit similar behavior, indicating that there is strong functionality in a region of periodic behavior. This functionality drops off as the power is increased.

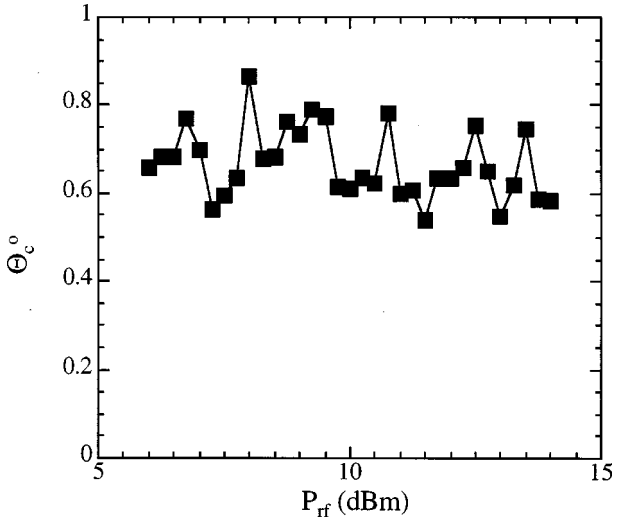

FIG. 9. This plot shows the value of the function statistic beyond linear (■) for the power sweep performed at 460.1 G and 3.0251 GHz, plotted against radio frequency power P_{rf}. The high values even where both the cross correlation and function statistic values are low (such as those above 10 dBm) indicate that there is some functionality in these states and that it is nonlinear in nature.

then digitized and processed. Both periodic and chaotic states have been observed over a wide parameter range. Each data set consists of a time series of the voltage signal from each probe. We investigate the relationship between the two time series by initially performing cross-correlation analysis to quantify the linear aspects of the relationship and then investigating the nonlinear aspects using the function statistics.

Figure 8 shows the linear correlation and nonlinear function statistic as a function of microwave excitation power for a power sweep performed at 460.1 Oe and 3.0251 GHz. Initially the signal-to-noise ratio is low but eventually the system evolves into a region of periodic states where both the cross-correlation and function statistic values are high. Both measures drop off as the states lose periodic structure and become more chaotic. We also show a plot of the function statistic beyond linear (Fig. 9), calculated using a least squares approximation for the linear model. The high value for the function statistic beyond linear indicates that the error in the linear model is greater than the attractor-wide noise scale σ. These results imply that there is a nonlinear component to the relationship in this parameter range.

We present results from another power sweep (performed at 2.9747 GHz and 449.9 Oe) in Fig. 10. The states in this power sweep produce periodic signals with similar spectra except in the region between 5.4 and 7.4 dBm. Here, the measured time series are quasiperiodic with two noncommensurate frequencies. The individual probes measure both frequencies but the relative intensities of the individual frequencies are different for each probe. The higher frequencies are more intense at the position monitored by the first probe, while the lower frequencies dominate the dynamics at the position monitored by the second probe. The linear cross correlation is much lower than the values for either of the nonlinear statistics at these powers. These results imply that there is some functionality in the power range that is highly nonlinear in nature. This is also an example of a system with functionality that cannot be characterized by the linear cross correlation and demonstrates the utility of the function statistic analysis. In order to further explore the behavior in this power range, we calculated both the function statistic and function statistic beyond linear for these states, interchanging

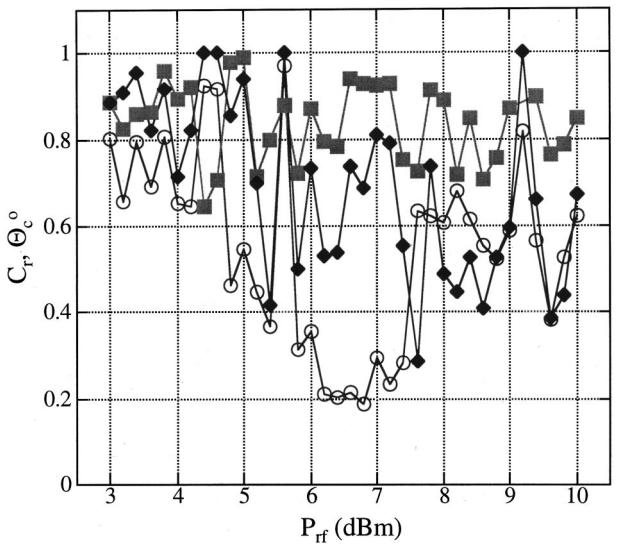

FIG. 10. A plot of the cross correlation (○), function statistic (◆), and function statistic beyond linear (gray ■) for a power sweep at 2.9747 GHz and 449.9 Oe, plotted against radio frequency power P_{rf}. In the region between 5.4–7.4 dBm, the two nonlinear statistics are higher than the linear cross correlation, indicating that the functionality in this region is nonlinear.

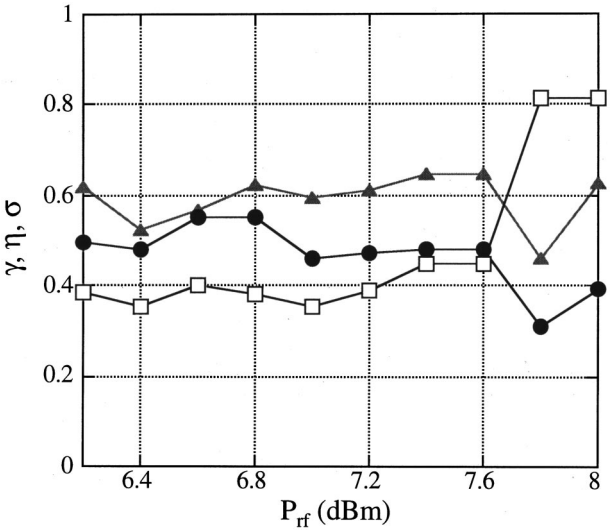

FIG. 11. Two different noise levels, γ (a measure of the stochastic noise level of the time series data) (gray ●) and σ (found during the calculation of function statistic) (□), are plotted with η (the variance of the residues from a least squares linear model) (●), against radio frequency power P_{rf}. σ is upper bounded by γ but the two noise statistics are close in value. η has more variation and is dependent on the strength of a linear fit between the attractors.

the source and target attractors. These values were very close to those previously determined (both for the function statistic and the function statistic beyond linear) and support the existence of an invertible function relating the time series.

We would like to determine if the results in Fig. 10 are caused by differences in the dynamics as driving power is increased or by different noise levels in the time series used to calculate the statistics. We use the Gamma statistic [22] as a test of the noise level. To find the Gamma statistic, we calculate the mean square distance from an arbitrary reference point to the pth nearest neighbor in the **X** attractor $[\Delta(p)]$ and the mean square distance from an arbitrary reference point to the pth nearest neighbor in the **Y** attractor $[\gamma(p)]$. We then plot $\gamma(p)$ as a function of $\Delta(p)$. As $p \rightarrow 0$, Steffansson, Konear, and Jones [22] show that $\gamma(p)$ approaches the variance of the noise level in the g time series. We can estimate the variance of the noise level from the y intercept of the $\gamma(p)$ vs $\Delta(p)$ plot.

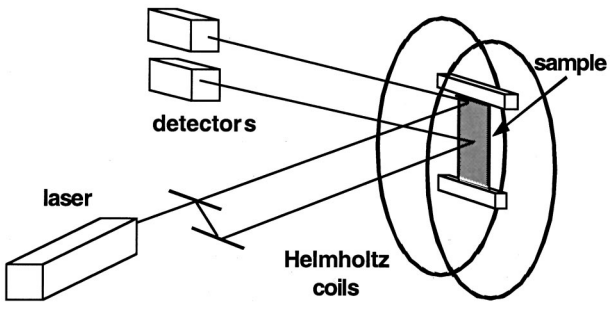

FIG. 12. Simple diagram of the driven magnetic ribbon experiment. The laser illuminates two spots on the ribbon, and the motion of these spots is used to detect the motion of the ribbon at the location of the spot.

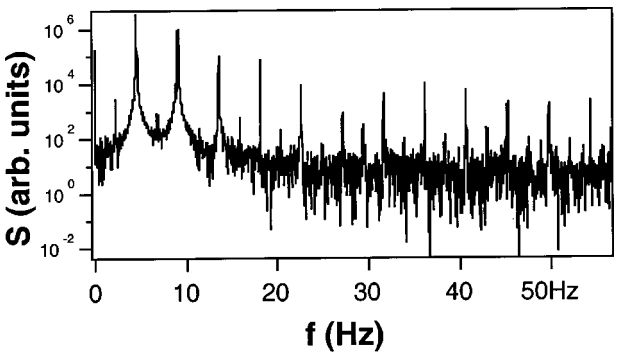

FIG. 13. Power spectrum S of the signal from the center of the ribbon when the ac driving field is 1.4 Oe. The time series has been sampled once per cycle of the driving frequency of 113 Hz.

We plot two noise measures, γ and σ, and the variance of the residues for a least squares linear model in Fig. 11. We plot the value of the γ statistic as defined above, which is a measure of the noise variance in the g time series. We also plot σ, which is a measure of the variance of a group of nearest neighbors on the **Y** attractor (calculated when we determine the function statistic). The γ statistic remains roughly the same size over the range of powers in Fig. 11, indicating that the noise levels in the different time series are roughly the same relative to the signal size. The differences seen between the statistics in Fig. 10 are not caused by differing noise levels. It is interesting to note that σ is roughly the same size as γ; the two different methods of determining a minimum length scale on the attractor **Y** give similar results. σ (calculated in the determination of the function statistic) is upper bounded by γ, indicating that this noise statistic is smaller than the underlying noise level in the data.

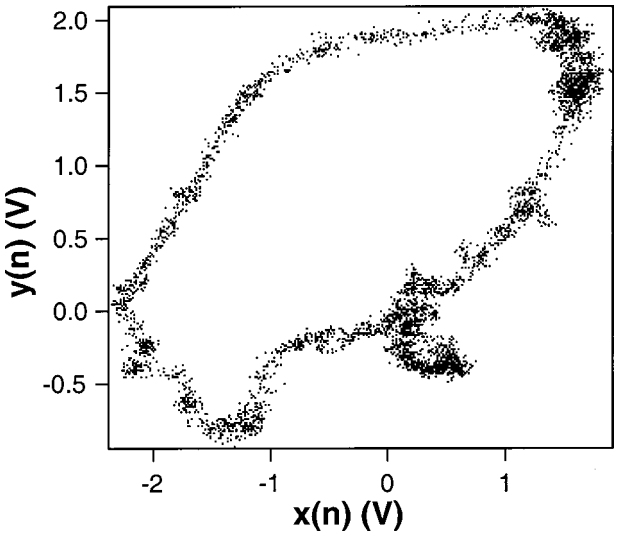

FIG. 14. Plot of one strobed time series $[x(n)]$ vs another strobed time series $[y(n)]$ taken with both laser spots at the center of the ribbon when the driving amplitude is 1.4 Oe. The two laser beams are at different angles, so the two time series are not the same.

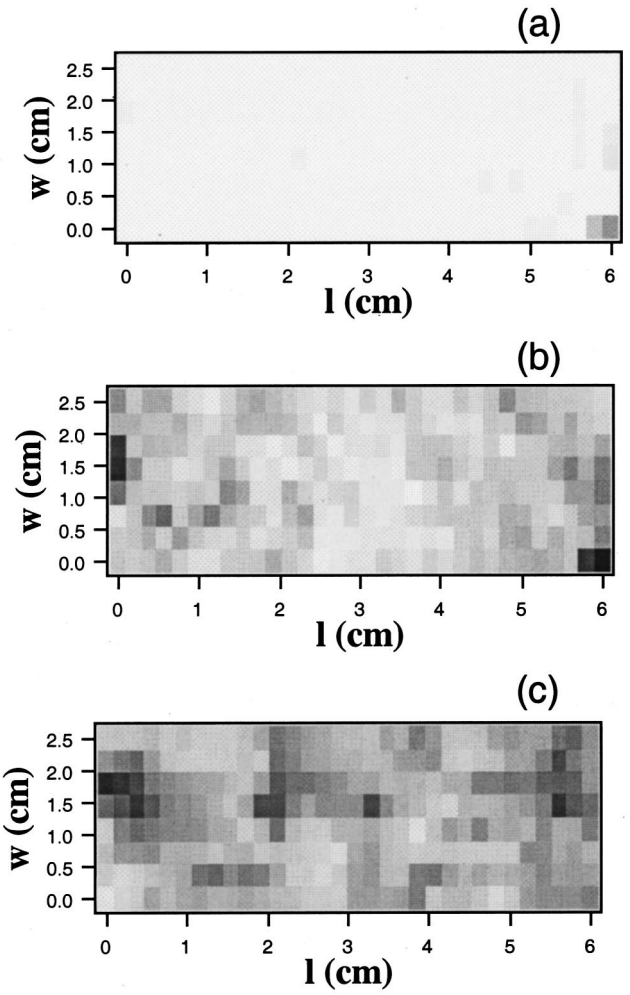

FIG. 15. (a) Plot of the function statistic beyond linear Θ_{c^0} over the surface of the ribbon, where one of the time series is measured at the center of the ribbon (when the drive amplitude is 1.4 Oe). White is equal to 1, while black is equal to 0. (b) Plot of the function statistic Θ_{c^0} over the surface of the ribbon. (c) Plot of the maximum value of the cross-correlation between detected time series from the ribbon.

IV. MAGNETOSTRICTIVE RIBBON EXPERIMENT

We also applied the statistics described above to data from an experiment involving a magnetostrictive metal ribbon. We suspended a ribbon of Metglass 2605 sc between a pair of Helmholtz coils. The top of the ribbon was rigidly clamped, while a 1.6 g mass was clamped across the bottom of the ribbon, allowing the bottom of the ribbon to swing freely. The ribbon was 25 mm wide, 60 mm long, and 1 mm thick. The Helmholtz coils produced a magnetic field in the plane of the ribbon. The magnetic field consisted of a 6.5 Oe dc field and an ac field that could be set to different magnitude and frequencies. The ac magnetic field couples to the domain walls in the ribbon to exert a time varying force on the ribbon. Figure 12 is a simple diagram of the experiment.

Two small spots (about 1 mm^2) on the ribbon were illuminated by a He-Ne laser. The ribbon surface was not smooth, so the spots produced diffuse reflections. The reflected light was focused on two small-area differential diode detectors, which compared the reflected beams to reference beams straight out of the laser in order to reduce noise from laser intensity modulations. Movement of the reflected beam across the detector produced a time varying signal proportional to the deflection of the ribbon at the spot illuminated by that spot. One laser spot was kept fixed in the center of the ribbon, while the other spot was scanned over the surface, so that two different signals were produced by the two detectors. Because each of the beams hit the ribbon at a different angle, different signals were produced even when both beams illuminated the same position.

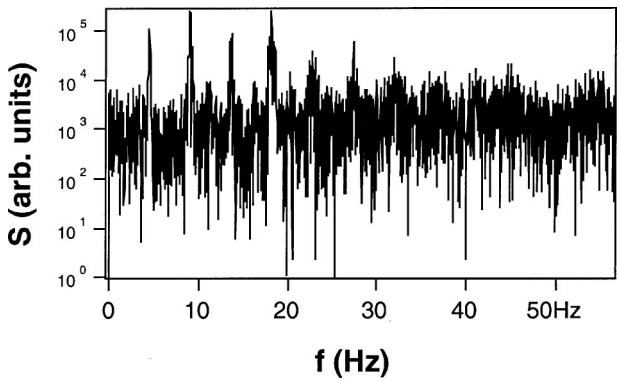

FIG. 16. Power spectrum S of the signal from the center of the ribbon when the ac driving field is 6.1 Oe. The time series has been sampled once per cycle of the driving frequency of 113 Hz.

The magnetization of the ribbon was coupled to its strain because the ribbon had a large magnetostriction. A magnetic field applied to the ribbon would alter the stiffness of the ribbon, as well as change its shape. The stiffness of the ribbon affected its mechanical response, so driving the ribbon with an ac magnetic field produced a highly nonlinear system.

We applied the function statistic, the function statistic beyond linear, and linear cross correlation to pairs of time series from the ribbon. Because the motion of the ribbon was highly nonlinear, it was not possible to tell by eye what the relation was (if any) between the two time series. Instead, we applied the statistics to determine what sort of relationships there might be. We drove the ribbon at an ac frequency of 113 Hz, which corresponds to a bending mode of the ribbon. We then sampled the time series signals from the two detectors every time the driving signal crossed zero in the positive direction. We then applied the statistics to these strobed time series.

A. Driving at 1.4 Oe

Figure 13 shows the power spectrum of one of these strobed time series when the ac magnetic field rms amplitude was 1.4 Oe. Figure 14 is a Poincare section obtained by plotting the strobed time series from one detector against the strobed time series from the other detector. The response of the ribbon appears to be quasiperiodic, responding at frequencies of 113 Hz, 4.5 Hz, and combinations of these frequencies.

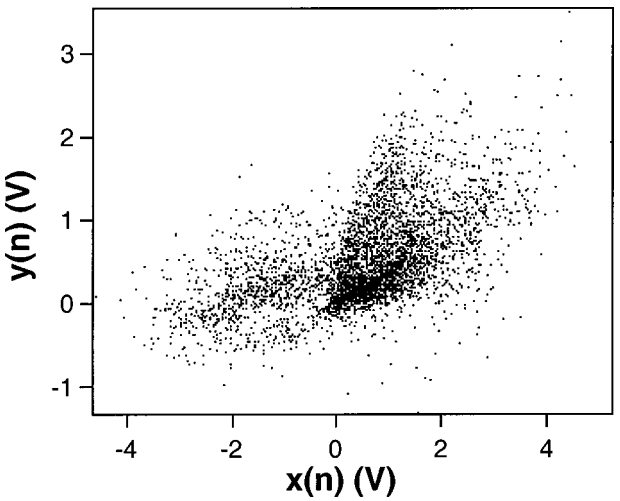

FIG. 17. Plot of one strobed time series $[x(n)]$ vs another strobed time series $[y(n)]$ taken with both laser spots at the center of the ribbon when the driving amplitude is 6.1 Oe. The two laser beams are at different angles, so the two time series are not the same.

In order to determine statistics, the laser spot that generated the time series labeled ''*y*'' was fixed at the center of the ribbon, while the time series labeled ''*x*'' was scanned over the ribbon. There were eight scans recorded along the narrow dimension of the ribbon and 32 scans recorded along the long dimension, for a total of 256 scans.

Figure 15(a) is a plot of the function statistic beyond linear Θ_{c0} obtained by comparing the strobed time series from the center of the ribbon to the strobed time series at other points at the ribbon. Each time series contained 2000 points embedded in five dimensions. White on the plot indicates a value of 1, while black indicates a value of 0. Θ_{c0} is near 1 over the entire surface of the ribbon, indicating that the relationship between the two embedded time series is not explained by a linear map. Either the relationship is nonlinear or there is no relation between the time series.

Figure 15(b) shows the value of the function statistic Θ_{c0} over the surface of the ribbon (where one of the time series is taken at the center of the ribbon). Θ_{c0} is slightly larger near the middle of the ribbon than near the ends, which suggests that it is easier to predict the motion at a point on the ribbon from a nearby point than from a distant point. We expect that we should be able to predict the motion of one point on the ribbon from the motion at another point because the ribbon is undergoing quasiperiodic motion, but noise can reduce the value of Θ_{c0}.

Figure 15(c) shows the maximum value of the cross correlation between the time series from the center of the ribbon and time series at other points. The cross correlation measures whether or not two signals are linearly related and also allows for a shift in time. The cross correlation between the time series is not very large for most points on the ribbon, so while Θ_{c0} shows that there is some predictability between time series from different points on the ribbon, the relationship between these time series is not simply linear. The cross correlation agrees with the function statistic beyond linear Θ_{c0}, which shows that any relation between time series is nonlinear.

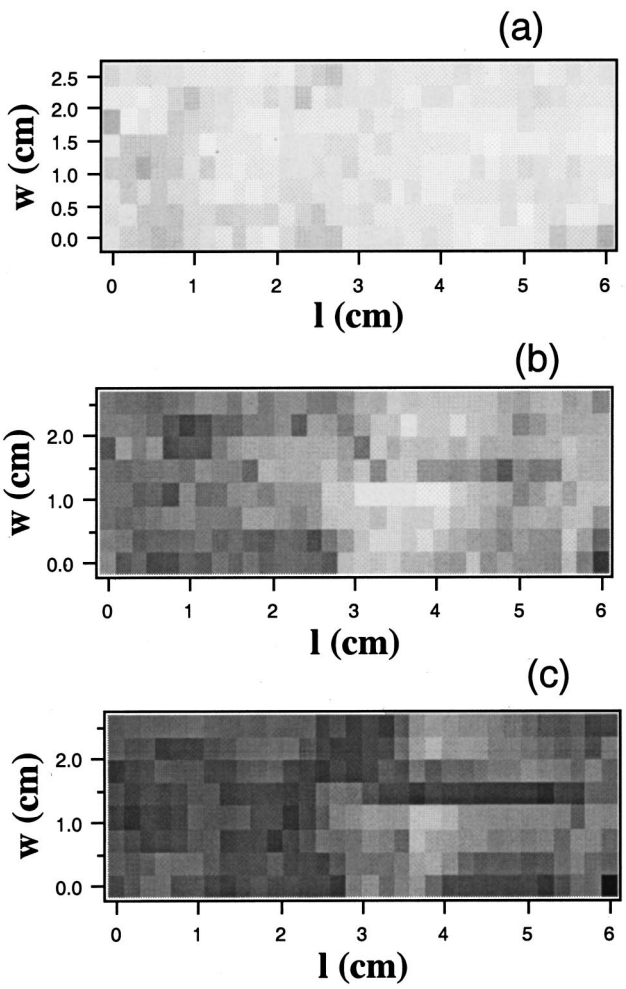

FIG. 18. (a) Plot of the function statistic beyond linear Θ_{c0} over the surface of the ribbon, where one of the time series is measured at the center of the ribbon (when the drive amplitude is 6.1 Oe). White is equal to 1, while black is equal to 0. (b) Plot of the function statistic Θ_{c0} over the surface of the ribbon. (c) Plot of the maximum value of the cross-correlation between detected time series from the ribbon.

B. Driving at 6.1 Oe

Figure 16 shows a power spectrum from a strobed time series when the ac magnetic field had an rms amplitude of 6.1 Oe. Spectral lines at multiples of 5 Hz are still present, but there is now also a large broadband background signal. In Fig. 17, the Poincare section for this data no longer appears to be quasiperiodic. The statistics for pairs of time series were computed as before, with an embedding dimension of 5.

The function statistic beyond linear Θ_{c0} in Fig. 18(a) is near 1 everywhere, suggesting that any relation between motion on different points on the ribbon is nonlinear. The function statistic Θ_{c0} in Fig. 18(b) appears to show two separate regions. Θ_{c0} is near 0 for regions near the top of the ribbon

and larger for regions near the bottom. The motion of the top half of the ribbon is not very predictable from the motion of the bottom half. The cross-correlation plot in Fig. 18(c) shows that the relation between motion on different parts of the ribbon is very nonlinear, except when the two parts of the ribbon are very close together.

This magnetic ribbon is being driven very hard, so it is unlikely that modeling of the motion of the ribbon for such large driving fields would be possible. All the information we can gain about the ribbon will come from statistics such as those used above. It is tempting to speculate whether or not the motion seen when the driving field is at 6.1 Oe is chaotic, but in our experience, attempting to calculate indicators of chaos such as Lyapunov exponents from experimental data is not yet very reliable at distinguishing chaotic motion from other complicated types of motion.

V. CONCLUSIONS

We have described a new way of quantifying the relationship between two time series and applied this technique to several experimental systems. This technique allows for the computation of a statistic that describes the strength of the relationship between two time series and also the intensity of the nonlinearity of any such relationship. Using this technique along with other linear and nonlinear techniques can help elucidate the relationship between time series and the underlying dynamics. Results from a variety of experiments show the utility of this analysis.

ACKNOWLEDGMENTS

The authors wish to thank D. King, W. Lechner, and J. Valenzi for technical assistance.

[1] H. Kantz and T. Schreiber, *Nonlinear Time Series Analysis* (Cambridge University Press, Cambridge, UK, 1997).
[2] C. Goodridge *et al.*, in Proceedings of the Fifth Experimental Chaos Conference, 1999, edited by M. Ding, W. L. Ditto, L. M. Pecora, and M. L. Spano.
[3] A. Aitta, G. Ahlers, and D. S. Cannell, Phys. Rev. Lett. **54**, 673 (1985).
[4] M. Dubois and P. Berge, J. Fluid Mech. **85**, 641 (1978).
[5] D. T. Kaplan, Physica D **73**, 38 (1994).
[6] L. Pecora, T. Carroll, and J. Heagy, Phys. Rev. E **52**, 3420 (1995).
[7] S. Schiff *et al.*, Phys. Rev. E **54**, 6708 (1996).
[8] The scale or limit or relevance is one possible measure of the stochastic noise level in the data.
[9] These measurements can be of position, temperature, voltage, or any other measurable quantity of the spatiotemporal system.
[10] H. D. I. Abarbanel, *Analysis of Observed Chaotic Data* (Springer-Verlag, New York, 1995).
[11] The attractors **X** and **Y** may have different dimension and time delay parameters.
[12] We define simultaneous points on the attractors to be vectors with identical first coordinates, since we do not require that the attractors have the same dimension or time delay.
[13] H. D. I. Abarbanel, N. F. Rulkov, and M. M. Sushchik, Phys. Rev. E **53**, 4528 (1996).
[14] J. Theiler, Phys. Rev. A **41**, 3038 (1990).
[15] R. Hogg and E. Tanis, *Probability and Statistical Inference* (Prentice-Hall, Upper Saddle River, NJ, 1997).
[16] H. Suhl, J. Phys. Chem. Solids **1**, 209 (1957).
[17] T. L. Carroll, L. M. Pecora, and F. J. Rachford, Phys. Rev. A **40**, 377 (1989).
[18] T. L. Carroll, L. M. Pecora, and F. J. Rachford, IEEE Trans. Magn. **27**, 5441 (1991).
[19] D. J. Mar *et al.*, J. Appl. Phys. **80**, 1878 (1996).
[20] D. J. Mar *et al.*, J. Appl. Phys. **81**, 5734 (1997).
[21] B. Lax and K. J. Button, *Microwave Ferrites and Ferrimagnetics* (McGraw-Hill, New York, 1962).
[22] A. Stefansson, N. Koncar, and A. J. Jones, Neural Comp. Appl. **5**, 131 (1997).